Slice-100K: A Multimodal Dataset for Extrusion-based 3D Printing

Anushrut Jignasu[1†] **Kelly O. Marshall**[2†] **Ankush Kumar Mishra**[1]
Lucas Nerone Rillo[1] **Baskar Ganapathysubramanian**[1] **Aditya Balu**[1]
Chinmay Hegde[2*] **Adarsh Krishnamurthy**[1*]

`{ajignasu | akmishra | lucasnr | baskarg | baditya | adarsh}@iastate.edu`
`{km3888 | chinmay.h}@nyu.edu`

[1]Iowa State University [2]New York University

[†]Equal contribution [*]Corresponding authors

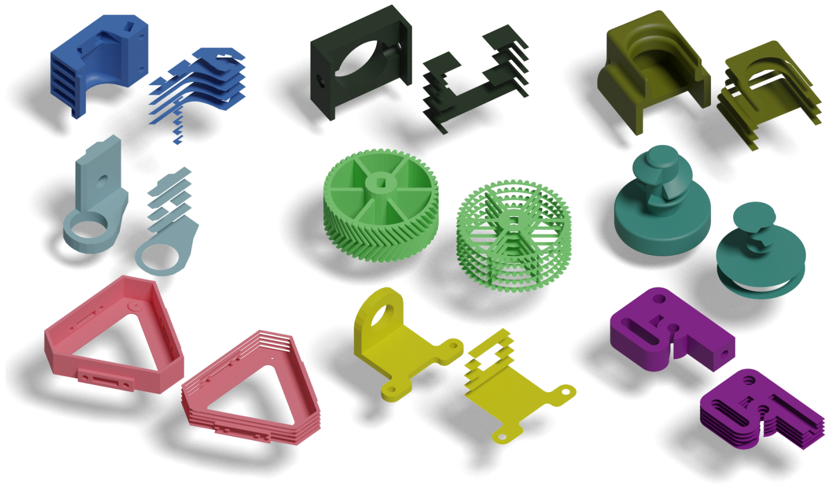

Figure 1: *The Slice-100K dataset consists of STL files and their G-code counterparts. Each pair here consists of STL (left) and its slices (right) for G-code.*

Abstract

G-code (Geometric code) or RS-274 is the most widely used computer numerical control (CNC) and 3D printing programming language. G-code provides machine instructions for the movement of the 3D printer, especially for the nozzle, stage, and extrusion of material for extrusion-based additive manufacturing. Currently, there does not exist a large repository of curated CAD models along with their corresponding G-code files for additive manufacturing. To address this issue, we present Slice-100K, a first-of-its-kind dataset of over 100,000 G-code files, along with their tessellated CAD model, LVIS (Large Vocabulary Instance Segmentation) categories, geometric properties, and renderings. We build our dataset from triangulated meshes derived from Objaverse-XL and Thingi10K datasets. We demonstrate the utility of this dataset by finetuning GPT-2 on a subset of the dataset for G-code translation from a legacy G-code format (Sailfish) to a more modern, widely used format (Marlin). Our dataset can be found here. Slice-100K will be the first step in developing a multimodal foundation model for digital manufacturing.

1 Introduction

In recent years, the integration of digital design and computer-aided manufacturing processes has led to groundbreaking innovations in the manufacturing sector [1, 2]. One of the most transformative technologies at this intersection is additive manufacturing or 3D printing, which enables the physical manufacturing of digital assets [3, 4]. 3D printing surpasses the limitations of traditional manufacturing techniques by enabling the creation of parts with complex geometric shapes [5, 6]. A commonly used 3D printing method is extrusion-based additive manufacturing [7, 8], often based on Fused Deposition Modeling (FDM) for manufacturing plastic or polymer parts. In this method, bits of thermoplastic material are sequentially extruded from a heated nozzle, which has three degrees of freedom. The nozzle moves in a flat 2D plane and builds up the desired shape layer-by-layer.

A typical 3D printing process begins with creating a 3D model of the part in a computer-aided design (CAD) program. This CAD model is then usually exported as a triangulated mesh file (for example, STL, PLY, or OBJ). The triangulated model is then "sliced" into multiple layers based on the resolution or the layer height of the 3D printer. Each layer is then converted into a sequence of programmatic instructions for the movement of the 3D printer's nozzle and extrusion of material along the boundary or "contour" of each layer. The instructions also include the movement of the nozzle and extrusion of material inside the contours or the "infill." These instructions are then directly sent to the 3D printer for physical manufacturing. The most common representation for storing this information is **G-code** (Geometric code) or RS-274, a computer numerical control (CNC) programming language. G-code provides machine instructions for the movement of the 3D printer, especially for the nozzle, stage, and extrusion of material for extrusion-based additive manufacturing. Although some extensions of G-code have been written to include basic abstractions such as for-loops, the vast majority of G-code in use consists mainly of low-level instructions that provide a sequence of commands to be carried out by the 3D printer.

Since 3D printing is a layered manufacturing process, it requires performing the slicing process. The slicing process operates on the entire object and splits it along the print direction (usually the Z-axis by default). Each layer is then used to generate the printer instructions for contour and infill. However, achieving high-quality fabricated models often requires manual tuning of the slicing software. The iterative improvement of a given G-code file to produce a 3D-printed model that exactly matches its CAD representation is a non-trivial challenge. In addition, there are several "flavors" of G-code files depending on the compatibility of the 3D printer's controller hardware. Due to the low-level nature of G-code, manually debugging a G-code file is cumbersome, if not impossible. Features such as line-level and layer-level natural language comments are infrequent. While custom solutions such as regular expression matching could be leveraged for correcting G-code, they fall under a rigid set of methods and are not generalizable.

In the last few years, while advances in AI have impacted various domains, their potential in computer-aided design (CAD) and cybermanufacturing remains largely untapped. Modern LLMs and Vision-Language Models (VLMs) could provide an avenue to realize this potential. The ability of LLMs to process, comprehend, and generate natural language descriptions, code, and other text data can be leveraged to interpret, generate, and manipulate G-code. LLMs for 3D shape modeling have been shown to enable operations on meshes [9, 10] and point clouds [11, 12]. G-code, with its unique language-based structure, presents distinct challenges for machine learning, mainly due to the context window limitations of current LLMs. Many existing deep-learning-based computer vision applications leverage 2D datasets (images), text descriptions, or a combination of such modalities for both supervised or self-supervised pre-training of foundation models (see Table 1). However, none of these datasets provide a curated avenue for training a manufacturing domain-specific foundation model.

To bridge this gap, we introduce Slice-100K, a curated multimodal dataset (see Figure 2 for reference) of G-code, CAD models, renderings, and geometric properties to facilitate the application of VLMs for additive manufacturing. We believe Slice-100K will encourage the research community to address new problems in the design and manufacturing space. Our dataset, built using models from Objaverse-XL and the Thingi10k dataset, encompasses a diverse range of 3D printable objects and provides a comprehensive resource for training a manufacturing domain-specific foundation model.

Contributions: This paper introduces Slice-100K, a multimodal dataset for manufacturing applications. The main features include a first-of-its-kind curated dataset of more than 100,000 G-code files along with their corresponding STL CAD files, renderings, LVIS (Large Vocabulary Instance

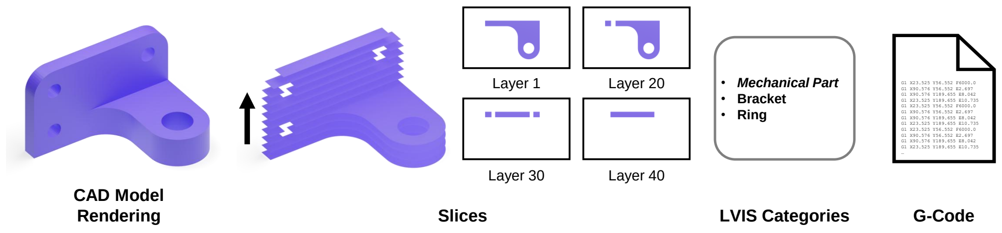

Figure 2: *Different data formats in Slice-100K. We build our dataset using CAD models (STL files) and their renderings. Furthermore, we slice these STL files to generate G-code (build direction shown by black arrow) and their categorical classifications.*

Segmentation) categories, and geometric properties. We demonstrate the utility of Slice-100K by evaluating existing LLMs for G-code geometric transformations. We also showcase a novel application of our dataset on LLM-based G-code flavor translation. We believe that this multimodal dataset will be the starting point for a foundation model in digital manufacturing.

2 Background and Related Work

G-code: G-code forms a crucial intermediary between digital design and physical manufacturing, providing an expressive language-based representation for 3D objects. For example, the most straightforward G-code command is `G1`, which directs the 3D printer to move its nozzle towards a spatial coordinate. This is usually followed by a coordinate in the form `Xaaa Yaaa`, where movement along the **X** and **Y** axes are given by a specific numeric value `aaa`. For extrusion-based 3D printers, a thermoplastic material is extruded from a heated nozzle that has three degrees of freedom. An example extrusion move is given by `G1 X50.6 Y36.2 E2.3`, where the nozzle moves 50.6 units along **X**, 36.2 units along **Y** and extrudes 2.3 units of material. Other commands instruct the printer to change settings, such as the material/ink feed rate, or perform more complex movements without extruding material.

Language Models for Code: LLMs have also been used for programming language analysis and code generation. Coding-focused LLMs are mainly trained on a mix of web-scraped data, coding repositories, and instructions and often surpass general-purpose LLMs in code-related tasks. Current research has lead to many such models [13–18]. Most notable ones include WizardCoder [18], Code Llama [19], and Instruct-CodeGen [16]. Codex [20] is an early model deployed under Github's Copilot feature and acts as an IDE assistant that can understand local code context, make suggestions, and generate entire blocks of code.

3D Datasets: The current research community has proposed and leveraged various 3D datasets [21–28]. Notable ones include Objaverse 1.0 [23] and Objaverse-XL [24], with the former consisting of over 800K 3D models with higher quality textures and geometry types (Table 1). The latter is a massive dataset of over 10 million objects gathered from various sources, including Thingi10K and GitHub repositories. The diversity of objects in terms of shapes and categories is an advantage for Objaverse-XL. Most of the datasets currently used by the research community provide a single modality (meshes or voxels), and some include text descriptions and renderings for visual supervision tasks. However, none of the currently available datasets provide curated assets for encouraging research in the manufacturing domain. The largest public G-code dataset we are aware of is the Greater G-code [29] dataset, which only contains 860 G-code files paired with their STL renderings.

LLMs and 3D Datasets: Language understanding methods have been applied in the 3D domain for a wide array of tasks including 3D captioning [26, 30], object grounding [11, 31], 3D conversation [32], and text-conditioned generation [9, 10, 10]. Recently, there has been a surge of interest in multimodal large language models (MLLMs). MLLMs combine the language-based reasoning and knowledge of LLMs with the ability to comprehend other data modalities. Vision-augmented LLMs [33–35] encode images into an LLM's embedding space. These methods have been subsequently extended to the 3D domain for different forms of 3D representation, such as point clouds [12, 36], and sparse outdoor LiDAR data [37]. Paschalidou et al. [38] use a transformer-based model (not LLM) to predict 3D objects in a scene autoregressively. 3DLLM [11] maps 3D scenes to a set of 2D image embeddings and uses a query-token embedding technique based on BLIP-2's Q-Former [34] to perform a diverse set of 3D-related tasks. GPT4Point [36] also leverages a similar Q-Former for point-

Table 1: *Comparison of different 3D multimodal datasets currently available.*

Dataset	Mesh	Renderings	Categories	G-code
ABC	✓	✓	✗	✗
ShapeNet	✓	✓	✓	✗
Thingi10K	✓	✓	✗	✗
Objaverse 1.0	✓	✓	✓	✗
Objaverse-XL	✓	✓	✓	✗
Slice-100K	✓	✓	✓	✓

text feature alignment. Chat3D [32] uses an object-centric 3D representation to train a 3D-LLM for dialogue. Feng et al. [39] does in-context learning on room layouts from the 3D-FRONT dataset [40]. PointBERT [41] did some early work on point-cloud representation learning with transformers. Fu et al. [30] align visual features from 3D scenes with text to finetune a LLaMa-2-chat-70B [42] model for scene understanding and question answering.

LLMs for Design and Manufacturing: Recent research has shown that natural language descriptions can be used for various tasks related to 3D printing, such as generating novel shapes [43–46], editing scenes [47], and reasoning about geometry in the volume space [48]. Makatura et al. [49] thoroughly examine GPT-4's suitability for automated design and manufacturing. Badini et al. [50] use ChatGPT to modify G-code, but they only alter the parameters in the G-code header. These modifications allow them to address common errors in the 3D printing process, such as warping, bed detachment, and stringing. Kulits et al. [51] train an LLM to autoregressively generate structured representations of simple 3D objects from the CLEVR dataset [52].

3 The Slice-100K Dataset

3.1 Data Collection Process

Dataset: We build our Slice-100K dataset using Objaverse-XL's openly available 3D dataset and Thingi10K dataset. Specifically, we download STL models from the Thingiverse branch of Objaverse-XL since these are solid models specifically designed to be additively manufacturable. We filter our models from the Thingi10K dataset using the following keywords: `num components = 1`, `is manifold`, and `is oriented`. A summary of our dataset is shown in Table 2, and we describe each data source below. In addition to providing STL models, our dataset includes renderings, descriptive captions, and detailed geometric properties. The metadata for each model is generated using Open3D, a library that facilitates the processing and analysis of 3D data. Key geometric properties such as vertex manifold, edge manifold, and vertex count are calculated and included in the dataset. These properties are essential for understanding the structural characteristics of the models and can be leveraged in various applications, such as model optimization and error detection in 3D printing.

The **Objaverse-XL** dataset comprises of 3D objects gathered from Github, Thingiverse, Smithsonian Institution, Polycam, and Sketchfab. We collect data from the Thingiverse subset of Objaverse-XL. Thingiverse is one of the largest online platforms consisting of user-generated digital designs and is particularly focused on 3D printable files, encouraging community interaction and collaboration. A majority of these files are provided in the STL format and are available under Creative Commons licenses. The models on Thingiverse cover a wide range of categories, including functional parts, artistic creations, and educational tools. This extensive and diverse collection makes it an invaluable resource for creating comprehensive datasets for additive manufacturing.

The **Thingi10K** dataset [27] is a collection of 10,000 3D models sourced from Thingiverse. It is curated explicitly for research purposes and provides a diverse set of models that are manifold and oriented, making them ideal for various computational geometry and 3D printing research applications. The dataset includes metadata and annotations that facilitate the development of machine learning models and other computational tools.

Table 2: *Composition of Slice-100K.*

Source	Number of Objects
Objaverse-XL (Thingiverse)	96,479
Thingi10k	3,589
Total	100,068

G-code Generation: The G-code generation process is a critical component of the Slice-100K dataset. We utilize PrusaSlicer's [53] command line functionality to slice all our models. Each model is sliced using two distinct G-code flavors—Sailfish and Marlin. Prusa's slicer is an open-source and widely-used slicing software that prepares 3D models for printing by converting them into G-code, which provides specific instructions for 3D printers. Additionally, it allows for extensive configuration options, allowing for fine-tuning of print settings such as layer height, infill density, and support structures. This flexibility ensures that the generated G-code is high quality and suitable for different 3D printers and printing conditions. Furthermore, to minimize our data footprint, we generate G-code files in the binary G-code (`.bgcode`) format, a functionality recently incorporated by Prusa's slicer. An important aspect of the slicing pipeline is the infill pattern selection, primarily due to its impact on total print time and structural properties of manufactured models. To encourage diversity among our G-code files with respect to structural properties, while slicing each STL file, we randomly select from four different infill patterns: (1) *Gyroid*: Empirically known to give equal strength across all directions and optimizes for a quicker print time; (2) *Honeycomb*: Uses a grid of hexagons, providing increased mechanical resistance, and non-crossing paths; (3) *Cubic*: Introduces crossing paths, potentially generating air-pockets; and (4) *Grid*: Uses a two-way checkerboard-like pattern for faster infill.

STL Renderings: To generate renderings of our STL files, we utilized Blender [54] rendering scripts made available by Objaverse-XL. We modified the scripts to generate a total of 10 views for each object - 6 orthogonal views (front, back, top, bottom, left, right) and 4 isometric views (captured from top four corners of a cube). Each object was rendered with a random color. These renderings were utilized for object category generation.

LVIS Object Categories: To generate the text category of each model in Slice-100K, we use the framework shown in Figure 3. For each model in our dataset, we assign the top 3 of the 1200+ LVIS (Large Vocabulary Instance Segmentation) categories [55]. This process helps enhance the utility of the dataset, enabling better categorization and facilitating more effective use in various research and development applications. For each CAD model, we generate multiple views using Blender. This step ensures comprehensive visual coverage of the model, capturing its geometry from various angles. The generated renderings serve as input to a pre-trained Vision-Language model to generate image embeddings. Specifically, we utilize a pre-trained CLIP-ViT-L-14 [56, 57] to obtain embeddings for each view. To integrate information from multiple views, we compute an average embedding for each object. This average embedding combines the features from all views into a single, unified representation, providing a comprehensive summary of the visual characteristics of the object.

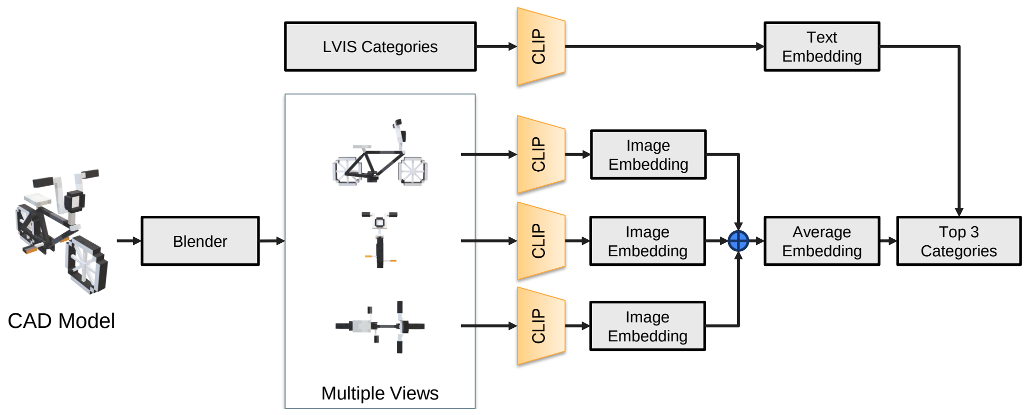

Figure 3: *Framework to generate the LVIS categories of the 3D objects.*

In parallel, we also process the 1200+ LVIS categories to obtain the text embeddings for all categories. Using the average embedding, we then match each object to the closest categories in the text embedding. By comparing the average embeddings, we identify the top 3 most relevant LVIS categories for each object in our dataset.

3.2 G-code Translation

G-code translation involves converting a G-code from one flavor to another while preserving the necessary context associated with each flavor and finding a correspondence between any two given flavors of G-code. We begin with G-code data in two different flavors, Sailfish and Marlin. Sailfish is a legacy G-code format that is not currently used by the 3D printing community. Marlin is a modern G-code format that has been heavily adopted, and in some cases, other G-code flavors are built on top of Marlin. Given this, we leverage our proposed dataset to finetune GPT-2 for the task of G-code translation from Sailfish to Marlin. G-code is inherently a low-level language, and for a task like translation, the quality of data being fed into an LLM has a significant impact on its performance. Keeping this in mind, we perform some data pre-processing to effectively maintain the context across lines of G-code.

3.2.1 Data Pre-Processing Methods

A major challenge in applying language-modeling-based techniques to G-code is the length of G-code files. While the G-code representation of a 3D shape can be separated into layers (which do not share information and hence be handled independently), this is still not sufficient, as a single layer can be over the token limit. This motivates methods for further splitting of G-code layers, allowing us to decompose mappings between G-code files into a series of mappings between smaller G-code portions. Crucially, these methods can be applied to different G-codes regardless of the variants they are written in while ensuring that the resulting pairs of G-code segments represent the same spatial semantics. To accomplish this, we first permute the contours in each G-code layer so that they have the same ordering. We then adaptively select portions to create matching pairs.

Contour Flipping: Let L_A and L_B be two G-code layers that use different flavors to represent the same 3D information. We can decompose each of these layers into a series of N contours $c_1^{(A)}, .., c_N^{(A)}$ and $c_1^{(B)}, .., c_N^{(B)}$, each represented using their respective flavor. Both sequences contain the same set of unique contours irrespective of the flavors. Because of this, we can define a bijective mapping $M : [N] \to [N]$ such that the contour $c_{M(i)}^{(B)}$ is equivalent to $c_i^{(A)}$.

The primary challenge in our preprocessing is to find this bijection, which, once found, allows us to re-order the contours of L_B so that $\forall i \in [N]$ we have that $c_i^{(B)}$ is equivalent to $c_i^{(B)}$. To determine M, we iterate over each contour $c_i^{(A)}$ in L_A and find its corresponding contour $c_{M(i)}^{(B)}$ in L_B. We consider two contours to be matching if there are specific commands which are included in both. More specifically, we define a method for representing a single line of G-code so that identical representations will indicate matching contours.

To minimize the possibility of a duplicate representation (that could lead to a false match), we base this criterion on G-code lines, which contain commands to extrude at specified coordinates. Other commands are disregarded as they are likely to be repeated throughout a file or contain syntax that differs across flavors. In contrast, extrusion locations are specified using floating point coordinates with several digits of precision, making it rare for the same point to appear in different contours. We further account for the possibility of duplicate locations by concatenating the line's coordinates with the next two lines in the contour where possible. If these following lines do not contain a location-specific extrusion command, we simply include in their place a token denoting an empty line. Together, this creates a string representation of each line that strips away flavor-specific syntax while including enough contextual information to prevent unwanted duplicates.

Using this consistent characterization of G-code lines allows us to match contours by simply finding a single pair of lines with the same representation. However, due to the length of G-code layers, it is highly inefficient to consider all possible pairs of lines when looking to match contours. To alleviate this, we pre-compute a lookup table for L_B. For each line of a contour $c_B^{(i)}$, the lookup table maps from the line representation to the index i. Then, when iterating over the contours of L_A, we compute the representation for each line and search the lookup table. If there is a match, then we add these indices to our bijection M. While this contour flipping method cannot be guaranteed to always find the correct bijection M due to variations amongst some contours, we find that it is highly reliable, producing aligned G-code for over 99.9% of the G-code layers in our dataset. We include pseudocode for our method in the Appendix (Algorithm 1).

Pair Creation: Given two G-code layers that have undergone contour flipping so that they have the same high-level semantic ordering, we can reasonably expect to divide them each into pairs of contiguous sections sharing the same 3D information. Because there are often commands included in one flavor but not the other, we cannot simply select portions of equal length and expect them to be translatable. Instead, we have to adaptively determine the cutoff points for each section.

Here we represent the layers as sequences of lines, with $L_A = \ell_1^{(A)}, ..., \ell_N^{(A)}$ and $L_B = \ell_1^{(B)}, ..., \ell_N^{(B)}$. Our goal of separating these layers into K matching chunks then amounts to finding pairs of delimiting line indices $(k_i^A, k_i^B)_{i=1}^K$ so that the resulting G-code segments $\ell_{k_i^A}^{(A)}, .., \ell_{k_{i+1}^A-1}^{(A)}$ and $\ell_{k_i^B}^{(B)}, .., \ell_{k_{i+1}^B-1}^{(B)}$ meet our requirements. In particular, we can ensure that the segments contain all the same content as long as the beginning and end lines of each language correspond to the same commands.

Our pair creation approach finds these matching line indices while respecting a maximum length parameter (see Algorithm 2 in Appendix). In short, we iteratively find index k_{i+1}^A by starting with a candidate value which is k_{i+1}^A plus the maximum length. We then try to find a matching line in L_B and, if successful, consider this a pair. If we cannot find a matching line for our candidate, we decrease the candidate line index by one and continue trying. We use a line representation similar to the one used for contour flipping to determine whether a pair of lines is matching.

Handling Extrusion Values: Through the previously described preprocessing methods we have been able to create pairs of G-code chunks which represent the same local information and can therefore be translated between. However, there is an additional non-local dependence that must be accounted for in the G-code extrusion values. In addition to telling the 3D printer where to move, a line of G-code also tells it how much material to extrude during this movement.

This is specified through an "E" command which states how much total material will have been extruded once that point is reached. For instance, if one line contains an E value of 3 and the next line has an E value of 3.1, then .1 units of material should be extruded during this movement. There are also specialized language-specific commands throughout a shape's G-code, which reset the total extrusion values to some smaller constant.

Because these values represent a cumulative sum of all material extruded up to that point starting from the most recent reset value, there is a non-locality element that must be addressed. During preprocessing, we amend each extrusion value by subtracting the previous line's extrusion value. We call this new value the relative extrusion. This represents only the amount of material that is to be extruded during this movement and allows for any translation model to learn a simple local mapping that is not dependent on other chunks. Finally, after generating the G-code in this relative form, we convert it back to its original format by computing its cumulative sum.

3.3 Geometric Transformation - Scaling

Scaling is considered to be a simple geometric transformation that results in a geometry being enlarged or shrunk depending on a scaling factor. We assume uniform scaling along all three principle directions (X, Y, and Z). We evaluate the ability of current chat-based LLMs to perform this simple linear transformation by providing them with a single layer of G-code and asking the prompts:

```
Can you scale the coordinates by a factor of 2 and give me the updated G-code?
Can you scale the entire layer by a factor of 2 and return the updated G-code?
```

At the time of our evaluation, we empirically arrived at the maximum number of lines of G-code an LLM in our test suite can accept before crossing their respective token limits. We leverage this fact to chunk the G-code before feeding it to an LLM.

3.4 Evaluation Metrics

To measure the quality of G-code generation models, we introduce an image-space IoU metric for G-code fidelity in comparison to ground truth. Because small errors in the produced G-code can lead to significant divergence in the produced shape, we find it insufficient to use a language-based metric for evaluation. Instead, we use an image-based measure of fidelity by rendering top-down images of each layer.

G-code Renderer: To the best of our knowledge, there does not currently exist open-source software that can programmatically generate renderings of G-code objects. To remedy this, we introduce and make public our Python-based tool for this purpose. The renderer generates a top-down rendering of an individual layer. This layer-wise approach is sensible for examining the 3D structure as it avoids occlusions and captures all relevant parts of the shape, even the infill that provides internal structural support for the part and may not be visible from the outside.

Image-Space IoU: We make use of our top-down renderer by defining an Intersection over Union (IoU) metric to capture similarity in image space rather than text space. To compute this loss for a layer of translated G-code, we render the layer as well as its ground-truth counterpart into top-down images and compute the 2D IoU. We can use this metric to quantify how well a G-code generation model produces accurate instructions for printing in the physical space. To account for the 3D-printing process's varying levels of sensitivity to error, we further define the IOU@k metric as the percentage of translated layers that have an IOU greater than k.

4 Experiments

We use Slice-100K for two tasks: evaluating current LLMs for G-code geometric transformation (*scaling*) and G-code flavor translation by finetuning GPT-2,

4.1 Evaluating Existing LLMs for G-code Geometric Transformations

We evaluate some of the existing chat-based LLMs (GPT series [58, 59], Claude [60], Llama-2 [42], and Starcoder [61]) for performing geometric transformations, specifically scaling a layer of the model. We find GPT-3.5 and GPT-4 struggle with the S-shape. Claude-2 is able to generate the outer contour of the cylinder and cube but struggles with infill generation for the cylinder and the S-shape. Furthermore, we see that the open-source models—Llama-2-70b and Starcoder—do not perform well. We visualize the G-code outputs from the various LLMs in our test suite and render them using Ultimaker's Cura [62] slicing software. Our results are shown in Figure 4.

`Expected`	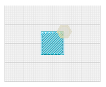	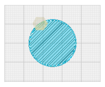	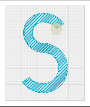
`GPT-3.5`	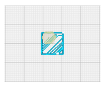	See Figure 8	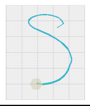
`GPT-4`	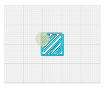	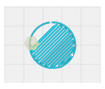	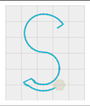
`Claude-2`	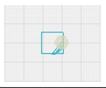	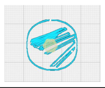	See Figure 10
`Llama-2-70b`	✗	See Figure 9	✗
`Starcoder`	✗	✗	✗

Figure 4: *G-code visualization for scaling operation on all LLMs. Expected G-code is shown in the top row. Please see the referenced figures in the Appendix for additional renderings.*

4.2 G-code Flavor Translation

For finetuning, we create a paired dataset of G-code chunks in each flavor using the preprocessing methods outlined in Section 3.2.1 using a maximum chunk size of 20 lines. We then finetune a lightweight GPT-2 model for translation using a next-token prediction loss. During inference, we do not have access to the ground-truth Marlin G-code, which would be needed to determine the cutoff lines for pair creation, so we instead split our Sailfish input into smaller chunks of fixed-length.

Table 3: *Performance of GPT-2 models finetuned for G-Code translation using differently sized subsets of SLICE-100k compared using IOU-based metrics. Training data reports the amount of Slice-100K data that models were finetuned on. The IOU metrics use our G-Code renderer to measure translation quality.*

Model	*Training Data*			*IOU Metrics*			
	Files	*Layers*	*Chunks*	**IOU@0.9**	**IOU@0.95**	**IOU@0.98**	**IOU@0.99**
GPT-2 Base	0	0	0	67	61	17	4
GPT-2$^{(1)}$	1	49	3933	95	88	71	27
GPT-2$^{(5)}$	5	545	13371	96	91	74	30
GPT-2$^{(25)}$	25	2298	51295	98	94	71	30

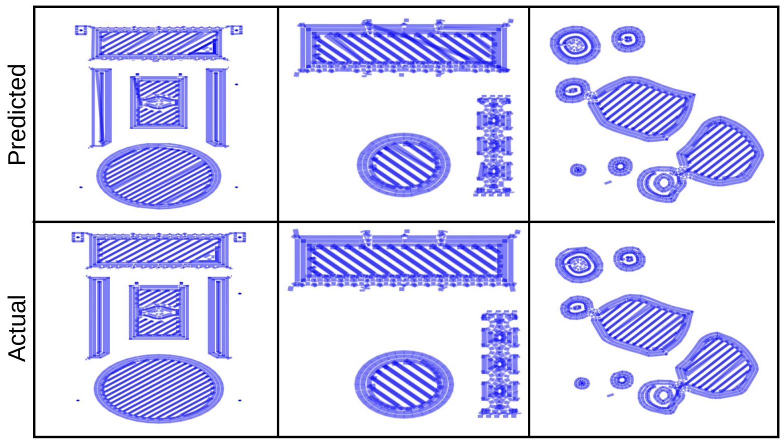

Figure 5: *Renderings of G-code layers predicted by a translation model finetuned on Slice-100K.*

Table 3 shows the results of performing finetuning on differently sized subsets of Slice-100K. We denote a GPT-2 model finetuned on n shapes from our dataset as GPT-2$^{(n)}$. Figure 5 shows example renderings of shapes that have undergone flavor translation by our GPT-2^5 model. We also include an example G-code that has been translated in the Appendix (Figure 11). We find that even finetuning on minimal subsets of our dataset leads to significantly enhanced G-code translation abilities. Increasing the amount of training data beyond just five G-code shapes finetuning ceases to yield improvements. We attribute this to our preprocessing methods, which reduce the complex translation task to a simple local mapping, thereby reducing the amount of data needed for learning.

5 Conclusion

In this paper, we presented Slice-100K, the first large-scale, curated dataset of over 100,000 G-code files, along with their corresponding STL CAD files, renderings, and geometric properties. This dataset addresses a significant gap in the availability of comprehensive resources for additive manufacturing. We showcase our dataset explorer in Figure 6 and various modalities offered by Slice-100K in Figure 7. Our evaluation demonstrated the usefulness of Slice-100K in utilizing existing language models for tasks such as G-code debugging, geometric transformations, and comprehension. Additionally, we introduced a novel application of using Slice-100K for LLM-based G-code flavor translation, showcasing the potential of our dataset in advancing the field. We believe that Slice-100K will serve as a foundational resource for future innovations in manufacturing, paving the way for the development of domain-specific foundation models.

Limitations: Despite these advancements, Slice-100K has certain limitations. One major challenge is the difficulty in verifying the LVIS categories of the models. Additionally, all models in Slice-100K were sliced along the default Z-direction. This uniform slicing approach may limit the dataset's applicability for research into multi-directional slicing techniques and their impact on manufacturing outcomes. Furthermore, we primarily focus on extrusion-based 3D printing among a plethora of additive manufacturing techniques. Addressing these limitations in future versions of the dataset will be crucial for further enhancing its utility and broadening its application scope.

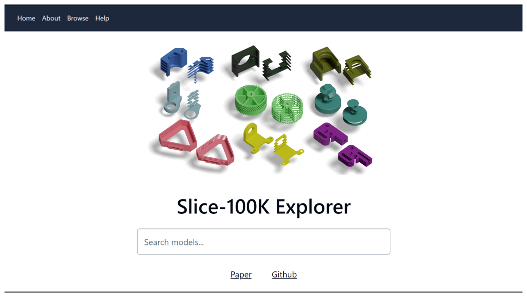

(a) *Home screen*

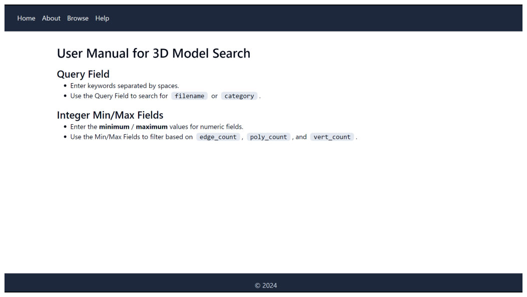

User Manual for 3D Model Search

Query Field

- Enter keywords separated by spaces.
- Use the Query Field to search for `filename` or `category` .

Integer Min/Max Fields

- Enter the **minimum** / **maximum** values for numeric fields.
- Use the Min/Max Fields to filter based on `edge_count` , `poly_count` , and `vert_count` .

© 2024

(b) *Search manual*

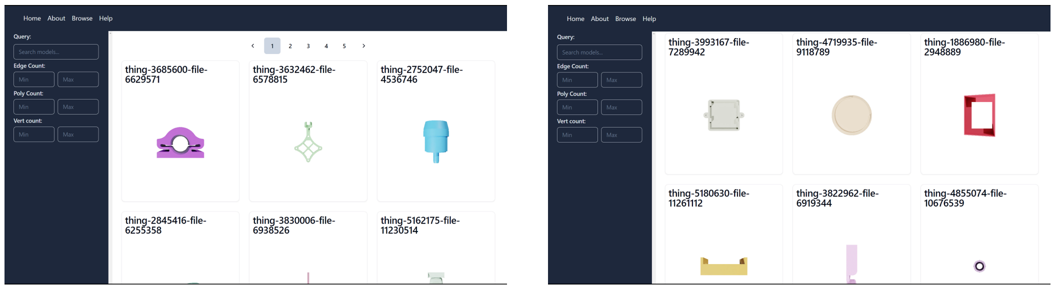
Home About Browse Help
Query:
Search models...
Edge Count:
Min
Max
Poly Count:
Min
Max
Vert count:
Min
Max
1 2 3 4 5
thing-3685600-file-6629571
thing-3632462-file-6578815
thing-2752047-file-4536746
thing-2845416-file-6255358
thing-3830006-file-6938526
thing-5162175-file-11230514
Home About Browse Help
Query:
Search models...
Edge Count:
Min
Max
Poly Count:
Min
Max
Vert count:
Min
Max
thing-3993167-file-7289942
thing-4719935-file-9118789
thing-1886980-file-2948889
thing-5180630-file-11261112
thing-3822962-file-6919344
thing-4855074-file-10676539

(c) *Model view*

Figure 6: *Dataset explorer screenshots: (a) Home screen, (b) Search manual, and (c) Model view.*

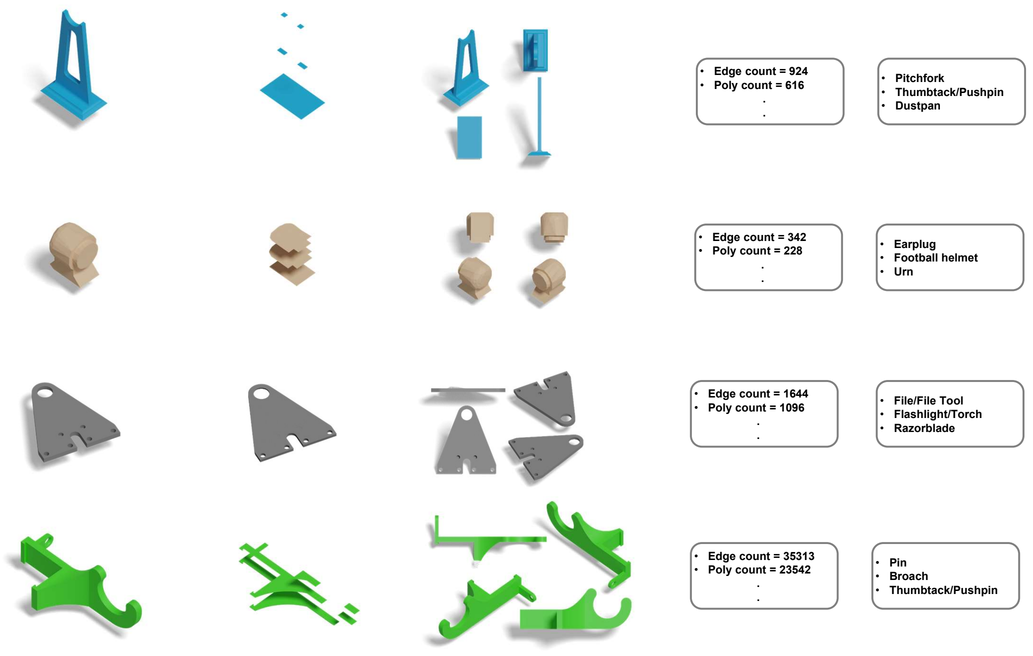

Figure 7: *Various modalities offered by Slice-100K.* ***First column*** *- CAD models,* ***Second column*** *- G-code,* ***Third column*** *- Renderings, and* ***Fourth and fifth columns*** *- Geometric properties and LVIS categories.*

Acknowledgements

This work was supported by the National Science Foundation under grant CMMI-2347623/2347624. We would like to thank the NVIDIA Corporation for providing GPUs for academic research.

References

[1] Vitor Alcácer and Virgilio Cruz-Machado. Scanning the industry 4.0: A literature review on technologies for manufacturing systems. *Engineering Science and Technology, an International Journal*, 2019.

[2] George Spanos, Glenn Daehn, John Allison, Elizabeth Bilitz, David Bourne, Jian Cao, Kester Clarke, Johnnie DeLoach Jr, Ed Herderick, John Lewandowski, et al. Metamorphic manufacturing: Shaping the future of on-demand components. Technical report, The Minerals Metals and Materials Society, Inc Pittsburgh United States, 2019.

[3] Alejandro Germán Frank, Lucas Santos Dalenogare, and Néstor Fabián Ayala. Industry 4.0 technologies: Implementation patterns in manufacturing companies. *International journal of production economics*, 210:15–26, 2019.

[4] Ugur M Dilberoglu, Bahar Gharehpapagh, Ulas Yaman, and Melik Dolen. The role of additive manufacturing in the era of Industry 4.0. *Procedia manufacturing*, 11:545–554, 2017.

[5] Tanisha Pereira, John V Kennedy, and Johan Potgieter. A comparison of traditional manufacturing vs additive manufacturing, the best method for the job. *Procedia Manufacturing*, 30:11–18, 2019.

[6] Charisios Achillas, Dimitrios Tzetzis, and Maria Olga Raimondo. Alternative production strategies based on the comparison of additive and traditional manufacturing technologies. *International Journal of Production Research*, 55(12):3497–3509, 2017.

[7] Ian Gibson, David W Rosen, Brent Stucker, Mahyar Khorasani, David Rosen, Brent Stucker, and Mahyar Khorasani. *Additive manufacturing technologies*, volume 17. Springer, 2021.

[8] Sanjay Kumar. *Additive manufacturing processes*. Springer, 2020.

[9] Yawar Siddiqui, Antonio Alliegro, Alexey Artemov, Tatiana Tommasi, Daniele Sirigatti, Vladislav Rosov, Angela Dai, and Matthias Nießner. MeshGPT: Generating triangle meshes with decoder-only transformers. *arXiv preprint arXiv:2311.15475*, 2023.

[10] Fukun Yin, Xin Chen, Chi Zhang, Biao Jiang, Zibo Zhao, Jiayuan Fan, Gang Yu, Taihao Li, and Tao Chen. ShapeGPT: 3D shape generation with a unified multi-modal language model. *CoRR*, abs/2311.17618, 2023. URL https://doi.org/10.48550/arXiv.2311.17618.

[11] Yining Hong, Haoyu Zhen, Peihao Chen, Shuhong Zheng, Yilun Du, Zhenfang Chen, and Chuang Gan. 3D-LLM: Injecting the 3D world into large language models. *arXiv*, 2023.

[12] Runsen Xu, Xiaolong Wang, Tai Wang, Yilun Chen, Jiangmiao Pang, and Dahua Lin. Pointllm: Empowering large language models to understand point clouds. *arXiv preprint arXiv:2308.16911*, 2023.

[13] Loubna Ben Allal, Raymond Li, Denis Kocetkov, Chenghao Mou, Christopher Akiki, Carlos Munoz Ferrandis, Niklas Muennighoff, Mayank Mishra, Alex Gu, Manan Dey, et al. Santacoder: don't reach for the stars! *arXiv preprint arXiv:2301.03988*, 2023.

[14] Fenia Christopoulou, Gerasimos Lampouras, Milan Gritta, Guchun Zhang, Yinpeng Guo, Zhongqi Li, Qi Zhang, Meng Xiao, Bo Shen, Lin Li, et al. Pangu-coder: Program synthesis with function-level language modeling. *arXiv preprint arXiv:2207.11280*, 2022.

[15] Bo Shen, Jiaxin Zhang, Taihong Chen, Daoguang Zan, Bing Geng, An Fu, Muhan Zeng, Ailun Yu, Jichuan Ji, Jingyang Zhao, et al. Pangu-coder2: Boosting large language models for code with ranking feedback. *arXiv preprint arXiv:2307.14936*, 2023.

[16] Sahil Chaudhary. instruct-codegen, 2024. URL https://huggingface.co/sahil2801/instruct-codegen-16B.

[17] Josh Achiam, Steven Adler, Sandhini Agarwal, Lama Ahmad, Ilge Akkaya, Florencia Leoni Aleman, Diogo Almeida, Janko Altenschmidt, Sam Altman, Shyamal Anadkat, et al. Gpt-4 technical report. *arXiv preprint arXiv:2303.08774*, 2023.

[18] Ziyang Luo, Can Xu, Pu Zhao, Qingfeng Sun, Xiubo Geng, Wenxiang Hu, Chongyang Tao, Jing Ma, Qingwei Lin, and Daxin Jiang. Wizardcoder: Empowering code large language models with evol-instruct. *arXiv preprint arXiv:2306.08568*, 2023.

[19] Baptiste Roziere, Jonas Gehring, Fabian Gloeckle, Sten Sootla, Itai Gat, Xiaoqing Ellen Tan, Yossi Adi, Jingyu Liu, Tal Remez, Jérémy Rapin, et al. Code llama: Open foundation models for code. *arXiv preprint arXiv:2308.12950*, 2023.

[20] Mark Chen, Jerry Tworek, Heewoo Jun, Qiming Yuan, Henrique Ponde de Oliveira Pinto, Jared Kaplan, Harri Edwards, Yuri Burda, Nicholas Joseph, Greg Brockman, et al. Evaluating large language models trained on code. *arXiv preprint arXiv:2107.03374*, 2021.

[21] Jasmine Collins, Shubham Goel, Kenan Deng, Achleshwar Luthra, Leon Xu, Erhan Gundogdu, Xi Zhang, Tomas F. Yago Vicente, Thomas Dideriksen, Himanshu Arora, Matthieu Guillaumin, and Jitendra Malik. ABO: dataset and benchmarks for real-world 3d object understanding. In *IEEE/CVF Conference on Computer Vision and Pattern Recognition, CVPR 2022, New Orleans, LA, USA, June 18-24, 2022*, pages 21094–21104. IEEE, 2022. doi: 10.1109/CVPR52688.2022.02045. URL https://doi.org/10.1109/CVPR52688.2022.02045.

[22] Angel X. Chang, Thomas A. Funkhouser, Leonidas J. Guibas, Pat Hanrahan, Qi-Xing Huang, Zimo Li, Silvio Savarese, Manolis Savva, Shuran Song, Hao Su, Jianxiong Xiao, Li Yi, and Fisher Yu. Shapenet: An information-rich 3d model repository. *CoRR*, abs/1512.03012, 2015. URL http://arxiv.org/abs/1512.03012.

[23] Matt Deitke, Dustin Schwenk, Jordi Salvador, Luca Weihs, Oscar Michel, Eli VanderBilt, Ludwig Schmidt, Kiana Ehsani, Aniruddha Kembhavi, and Ali Farhadi. Objaverse: A universe of annotated 3D objects. In *IEEE/CVF Conference on Computer Vision and Pattern Recognition, CVPR*, pages 13142–13153. IEEE, 2023. URL https://doi.org/10.1109/CVPR52729.2023.01263.

[24] Matt Deitke, Ruoshi Liu, Matthew Wallingford, Huong Ngo, Oscar Michel, Aditya Kusupati, Alan Fan, Christian Laforte, Vikram Voleti, Samir Yitzhak Gadre, Eli VanderBilt, Aniruddha Kembhavi, Carl Vondrick, Georgia Gkioxari, Kiana Ehsani, Ludwig Schmidt, and Ali Farhadi. Objaverse-XL: A universe of 10M+ 3D objects. In *Advances in Neural Information Processing Systems*, 2023.

[25] Sebastian Koch, Albert Matveev, Zhongshi Jiang, Francis Williams, Alexey Artemov, Evgeny Burnaev, Marc Alexa, Denis Zorin, and Daniele Panozzo. Abc: A big cad model dataset for geometric deep learning. In *Proceedings of the IEEE/CVF conference on computer vision and pattern recognition*, pages 9601–9611, 2019.

[26] Tiange Luo, Chris Rockwell, Honglak Lee, and Justin Johnson. Scalable 3D captioning with pretrained models. *arXiv preprint arXiv:2306.07279*, 2023.

[27] Qingnan Zhou and Alec Jacobson. Thingi10k: A dataset of 10,000 3D-printing models. *arXiv preprint arXiv:1605.04797*, 2016.

[28] Mikaela Angelina Uy, Quang-Hieu Pham, Binh-Son Hua, Thanh Nguyen, and Sai-Kit Yeung. Revisiting point cloud classification: A new benchmark dataset and classification model on real-world data. In *Proceedings of the IEEE/CVF international conference on computer vision*, pages 1588–1597, 2019.

[29] Alayt Issak. Greater G-code. Kaggle dataset repository, 2022. URL https://doi.org/10.34740/kaggle/dsv/3970532.

[30] Rao Fu, Jingyu Liu, Xilun Chen, Yixin Nie, and Wenhan Xiong. Scene-llm: Extending language model for 3d visual understanding and reasoning. *arXiv preprint arXiv:2403.11401*, 2024.

[31] Panos Achlioptas, Ahmed Abdelreheem, Fei Xia, Mohamed Elhoseiny, and Leonidas J. Guibas. ReferIt3D: Neural listeners for fine-grained 3D object identification in real-world scenes. In *European Conference on Computer Vision (ECCV)*, volume 12346, pages 422–440. Springer, 2020.

[32] Zehan Wang, Haifeng Huang, Yang Zhao, Ziang Zhang, and Zhou Zhao. Chat-3D: Data-efficiently tuning large language model for universal dialogue of 3D scenes. *CoRR*, abs/2308.08769, 2023. doi: 10.48550/ARXIV.2308.08769. URL https://doi.org/10.48550/arXiv.2308.08769.

[33] Haotian Liu, Chunyuan Li, Qingyang Wu, and Yong Jae Lee. Visual instruction tuning. In *NeurIPS*, 2023.

[34] Junnan Li, Dongxu Li, Silvio Savarese, and Steven Hoi. BLIP-2: Bootstrapping language-image pre-training with frozen image encoders and large language models, 2023.

[35] Deyao Zhu, Jun Chen, Xiaoqian Shen, Xiang Li, and Mohamed Elhoseiny. MiniGPT-4: Enhancing vision-language understanding with advanced large language models. *arXiv preprint arXiv:2304.10592*, 2023.

[36] Zhangyang Qi, Ye Fang, Zeyi Sun, Xiaoyang Wu, Tong Wu, Jiaqi Wang, Dahua Lin, and Hengshuang Zhao. Gpt4point: A unified framework for point-language understanding and generation. In *CVPR*, 2024.

[37] Senqiao Yang, Jiaming Liu, Ray Zhang, Mingjie Pan, Zoey Guo, Xiaoqi Li, Zehui Chen, Peng Gao, Yandong Guo, and Shanghang Zhang. Lidar-llm: Exploring the potential of large language models for 3d lidar understanding. *CoRR*, abs/2312.14074, 2023. doi: 10.48550/ARXIV.2312.14074. URL https://doi.org/10.48550/arXiv.2312.14074.

[38] Despoina Paschalidou, Amlan Kar, Maria Shugrina, Karsten Kreis, Andreas Geiger, and Sanja Fidler. Atiss: Autoregressive transformers for indoor scene synthesis. In *Advances in Neural Information Processing Systems (NeurIPS)*, 2021.

[39] Weixi Feng, Wanrong Zhu, Tsu jui Fu, Varun Jampani, Arjun Akula, Xuehai He, Sugato Basu, Xin Eric Wang, and William Yang Wang. Layoutgpt: Compositional visual planning and generation with large language models, 2023.

[40] Huan Fu, Bowen Cai, Lin Gao, Ling-Xiao Zhang, Jiaming Wang, Cao Li, Qixun Zeng, Chengyue Sun, Rongfei Jia, Binqiang Zhao, et al. 3d-front: 3d furnished rooms with layouts and semantics. In *Proceedings of the IEEE/CVF International Conference on Computer Vision*, pages 10933–10942, 2021.

[41] Xumin Yu, Lulu Tang, Yongming Rao, Tiejun Huang, Jie Zhou, and Jiwen Lu. Point-BERT: Pre-training 3D point cloud transformers with masked point modeling. In *IEEE/CVF Conference on Computer Vision and Pattern Recognition, CVPR*, pages 19291–19300. IEEE, 2022. URL https://doi.org/10.1109/CVPR52688.2022.01871.

[42] Hugo Touvron, Thibaut Lavril, Gautier Izacard, Xavier Martinet, Marie-Anne Lachaux, Timothée Lacroix, Baptiste Rozière, Naman Goyal, Eric Hambro, Faisal Azhar, Aurelien Rodriguez, Armand Joulin, Edouard Grave, and Guillaume Lample. LLaMA: Open and efficient foundation language models, 2023.

[43] Aditya Sanghi, Hang Chu, Joseph G Lambourne, Ye Wang, Chin-Yi Cheng, Marco Fumero, and Kamal Rahimi Malekshan. Clip-forge: Towards zero-shot text-to-shape generation. In *Proceedings of the IEEE/CVF Conference on Computer Vision and Pattern Recognition*, pages 18603–18613, 2022.

[44] Kelly O Marshall, Minh Pham, Ameya Joshi, Anushrut Jignasu, Aditya Balu, and Adarsh Krishnamurthy Chinmay Hegde. Zeroforge: Feedforward text-to-shape without 3d supervision. *arXiv preprint arXiv:2306.08183*, 2023.

[45] Ajay Jain, Ben Mildenhall, Jonathan T Barron, Pieter Abbeel, and Ben Poole. Zero-shot text-guided object generation with dream fields. In *Proceedings of the IEEE/CVF Conference on Computer Vision and Pattern Recognition*, pages 867–876, 2022.

[46] Chen-Hsuan Lin, Jun Gao, Luming Tang, Towaki Takikawa, Xiaohui Zeng, Xun Huang, Karsten Kreis, Sanja Fidler, Ming-Yu Liu, and Tsung-Yi Lin. Magic3d: High-resolution text-to-3d content creation. In *Proceedings of the IEEE/CVF Conference on Computer Vision and Pattern Recognition*, pages 300–309, 2023.

[47] Ayaan Haque, Matthew Tancik, Alexei A Efros, Aleksander Holynski, and Angjoo Kanazawa. Instruct-nerf2nerf: Editing 3d scenes with instructions. *arXiv preprint arXiv:2303.12789*, 2023.

[48] Justin Kerr, Chung Min Kim, Ken Goldberg, Angjoo Kanazawa, and Matthew Tancik. Lerf: Language embedded radiance fields. *arXiv preprint arXiv:2303.09553*, 2023.

[49] Liane Makatura, Michael Foshey, Bohan Wang, Felix HähnLein, Pingchuan Ma, Bolei Deng, Megan Tjandrasuwita, Andrew Spielberg, Crystal Elaine Owens, Peter Yichen Chen, et al. How can large language models help humans in design and manufacturing? *arXiv preprint arXiv:2307.14377*, 2023.

[50] Silvia Badini, Stefano Regondi, Emanuele Frontoni, and Raffaele Pugliese. Assessing the capabilities of chatgpt to improve additive manufacturing troubleshooting. *Advanced Industrial and Engineering Polymer Research*, 2023.

[51] Peter Kulits, Haiwen Feng, Weiyang Liu, Victoria Abrevaya, and Michael J. Black. Re-thinking inverse graphics with large language models, 2024.

[52] Justin Johnson, Bharath Hariharan, Laurens van der Maaten, Li Fei-Fei, C. Lawrence Zitnick, and Ross Girshick. Clevr: A diagnostic dataset for compositional language and elementary visual reasoning. In *Proceedings of the IEEE Conference on Computer Vision and Pattern Recognition (CVPR)*, July 2017.

[53] PrusaSlicer. Prusa, 2024. URL `https://www.prusa3d.com/page/prusaslicer_424/`.

[54] Blender Org. Blender, 2024. URL `https://www.blender.org/`.

[55] Agrim Gupta, Piotr Dollar, and Ross Girshick. Lvis: A dataset for large vocabulary instance segmentation. In *Proceedings of the IEEE/CVF conference on Computer Vision and Pattern Recognition (CVPR)*, pages 5356–5364, 2019.

[56] Alec Radford, Jong Wook Kim, Chris Hallacy, Aditya Ramesh, Gabriel Goh, Sandhini Agarwal, Girish Sastry, Amanda Askell, Pamela Mishkin, Jack Clark, et al. Learning transferable visual models from natural language supervision. In *International conference on machine learning*, pages 8748–8763. PMLR, 2021.

[57] OpenAI. CLIP-ViT-L/14, 2024. URL `https://huggingface.co/openai/clip-vit-large-patch14`.

[58] Tom B. Brown, Benjamin Mann, Nick Ryder, Melanie Subbiah, Jared Kaplan, Prafulla Dhariwal, Arvind Neelakantan, Pranav Shyam, Girish Sastry, Amanda Askell, Sandhini Agarwal, Ariel Herbert-Voss, Gretchen Krueger, Tom Henighan, Rewon Child, Aditya Ramesh, Daniel M. Ziegler, Jeffrey Wu, Clemens Winter, Christopher Hesse, Mark Chen, Eric Sigler, Mateusz Litwin, Scott Gray, Benjamin Chess, Jack Clark, Christopher Berner, Sam McCandlish, Alec Radford, Ilya Sutskever, and Dario Amodei. Language models are few-shot learners, 2020.

[59] OpenAI. GPT-4 technical report, 2023.

[60] Anthropic. Claude, 2023. URL `https://www.anthropic.com/product`.

[61] Raymond Li, Loubna Ben Allal, Yangtian Zi, Niklas Muennighoff, Denis Kocetkov, Chenghao Mou, Marc Marone, Christopher Akiki, Jia Li, Jenny Chim, Qian Liu, Evgenii Zheltonozhskii, Terry Yue Zhuo, Thomas Wang, Olivier Dehaene, Mishig Davaadorj, Joel Lamy-Poirier, João Monteiro, Oleh Shliazhko, Nicolas Gontier, Nicholas Meade, Armel Zebaze, Ming-Ho Yee, Logesh Kumar Umapathi, Jian Zhu, Benjamin Lipkin, Muhtasham Oblokulov, Zhiruo Wang, Rudra Murthy, Jason Stillerman, Siva Sankalp Patel, Dmitry Abulkhanov, Marco Zocca, Manan Dey, Zhihan Zhang, Nour Fahmy, Urvashi Bhattacharyya, Wenhao Yu, Swayam Singh, Sasha Luccioni, Paulo Villegas, Maxim Kunakov, Fedor Zhdanov, Manuel Romero, Tony Lee, Nadav Timor, Jennifer Ding, Claire Schlesinger, Hailey Schoelkopf, Jan Ebert, Tri Dao, Mayank Mishra, Alex Gu, Jennifer Robinson, Carolyn Jane Anderson, Brendan Dolan-Gavitt, Danish Contractor, Siva Reddy, Daniel Fried, Dzmitry Bahdanau, Yacine Jernite, Carlos Muñoz Ferrandis, Sean Hughes, Thomas Wolf, Arjun Guha, Leandro von Werra, and Harm de Vries. StarCoder: May the source be with you!, 2023.

[62] Ultimaker. Cura, 2024. URL `https://ultimaker.com/software/ultimaker-cura/`.

Checklist

1. For all authors...
   (a) Do the main claims made in the abstract and introduction accurately reflect the paper's contributions and scope? [Yes]
   (b) Did you describe the limitations of your work? [Yes]
   (c) Did you discuss any potential negative societal impacts of your work? [N/A] Since the data generated involves fundamental science, the negative impact it has on society is of a similar nature to any fundamental manufacturing technology itself.
   (d) Have you read the ethics review guidelines and ensured that your paper conforms to them? [Yes]
2. If you are including theoretical results...
   (a) Did you state the full set of assumptions of all theoretical results? [N/A]
   (b) Did you include complete proofs of all theoretical results? [N/A]
3. If you ran experiments (e.g. for benchmarks)...
   (a) Did you include the code, data, and instructions needed to reproduce the main experimental results (either in the supplemental material or as a URL)? [Yes] Material will be shared with reviewers.
   (b) Did you specify all the training details (e.g., data splits, hyperparameters, how they were chosen)? [Yes] See supplementary material.
   (c) Did you report error bars (e.g., with respect to the random seed after running experiments multiple times)? [Yes] See supplementary material.
   (d) Did you include the total amount of compute and the type of resources used (e.g., type of GPUs, internal cluster, or cloud provider)? [Yes] See supplementary material.
4. If you are using existing assets (e.g., code, data, models) or curating/releasing new assets...
   (a) If your work uses existing assets, did you cite the creators? [Yes]
   (b) Did you mention the license of the assets? [Yes]
   (c) Did you include any new assets either in the supplemental material or as a URL? [No]
   (d) Did you discuss whether and how consent was obtained from people whose data you're using/curating? [Yes] See supplementary material.
   (e) Did you discuss whether the data you are using/curating contains personally identifiable information or offensive content? [Yes] See supplementary material.
5. If you used crowdsourcing or conducted research with human subjects...
   (a) Did you include the full text of instructions given to participants and screenshots, if applicable? [N/A]
   (b) Did you describe any potential participant risks, with links to Institutional Review Board (IRB) approvals, if applicable? [N/A]
   (c) Did you include the estimated hourly wage paid to participants and the total amount spent on participant compensation? [N/A]

A Appendix

Algorithm 1 Contour Flipping

```
procedure ContourFlip($LayerA, LayerB$)
    $ContoursA \leftarrow ContourSplit(LayerA)$
    $ContoursB \leftarrow ContourSplit(LayerB)$
    $Lookup \leftarrow HashMap()$                          ▷ Create hash index of contours in Layer B
    for $c \leftarrow 1$ to length($ContoursB$) do
        for $i \leftarrow 1$ to length($ContoursB[c]$) do
            $line_i \leftarrow representation(ContoursB[c][i])$
            if $line_i \in Lookup$ and $Lookup[line_i] \neq i$ then
                Delete $Lookup[line_i]$
            else
                $Lookup[line_i] \leftarrow c$
            end if
        end for
    end for
    $Mapping \leftarrow HashMap()$                          ▷ Find bijection between layers
    for $c_A \leftarrow 1$ to length($ContoursA$) do
        for $i \leftarrow 1$ to length($ContoursA[c_A]$) do
            $line_i \leftarrow representation(ContoursA[c_A][i])$
            if $line_i \in Lookup$ then
                $c_B \leftarrow Lookup[line_i]$
                $Mapping[c_B] \leftarrow c_A$
            end if
        end for
    end for
    $FlippedB \leftarrow Array[$length$(ContoursB[c_A])]$
    for $i \leftarrow 1$ to length($ContoursB$) do
        $FlippedB[Mapping[c_i]] \leftarrow ContoursB[i]$
    end for
    return $LayerA, FlippedB$
end procedure
```

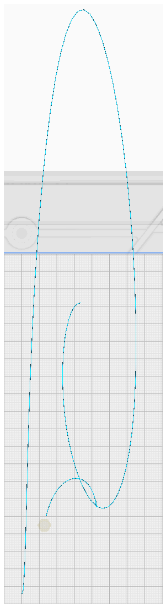

Figure 8: *`GPT-3.5` outlier case for scaling a cylinder.*

Algorithm 2 Pair Creation

```
procedure PAIR CREATION($LayerA, LayerB, maxLength$)
    $start_i, start_j \leftarrow 0, 0$
    $end_i \leftarrow maxLength$
    $pairs \leftarrow List()$
    while $start_i <=$ length($LayerA$) do
        $end_j \leftarrow start_j + 1$
        $found \leftarrow False$
        while $\neg found$ and $(end_j - start_j) \leq maxLength$ do
            if $representation(LayerA[end_i]) = representation(LayerB[end_j])$ then
                $found \leftarrow True$
            end if
            $end_j = end_j + 1$
        end while
        if $found$ then                                  ▷ Add matching pair of chunks to dataset
            $chunk_a \leftarrow LayerA[start_i : end_i]$
            $chunk_b \leftarrow LayerB[start_j : end_j]$
            $pairs.append((chunk_a, chunk_b))$
        else
            $end_i = end_i - 1$       ▷ Could not find a line matching line $end_i$, try a smaller chunk
        end if
    end while
    return $LayerA, FlippedB$
end procedure
```

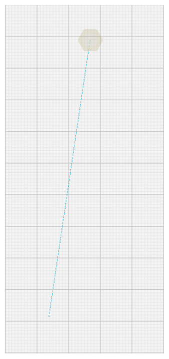

Figure 9: *`Llama-2-70b` outlier case for scaling a cylinder*

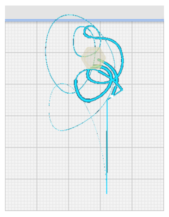

Figure 10: *`Claude-2` outlier case for Scaling S-shape.*

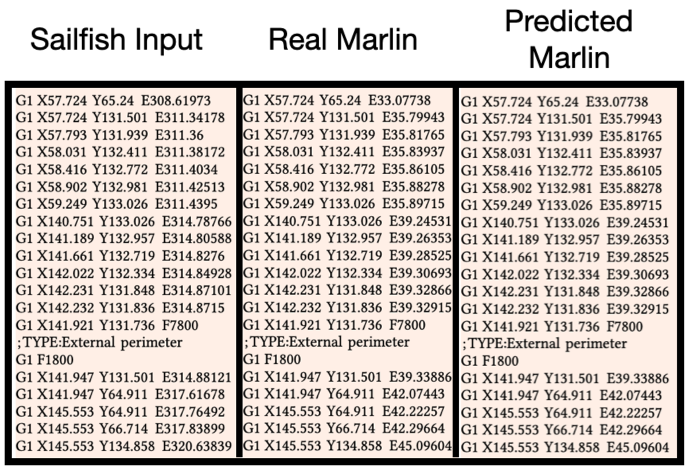

Sailfish Input	Real Marlin	Predicted Marlin
G1 X57.724 Y65.24 E308.61973	G1 X57.724 Y65.24 E33.07738	G1 X57.724 Y65.24 E33.07738
G1 X57.724 Y131.501 E311.34178	G1 X57.724 Y131.501 E35.79943	G1 X57.724 Y131.501 E35.79943
G1 X57.793 Y131.939 E311.36	G1 X57.793 Y131.939 E35.81765	G1 X57.793 Y131.939 E35.81765
G1 X58.031 Y132.411 E311.38172	G1 X58.031 Y132.411 E35.83937	G1 X58.031 Y132.411 E35.83937
G1 X58.416 Y132.772 E311.4034	G1 X58.416 Y132.772 E35.86105	G1 X58.416 Y132.772 E35.86105
G1 X58.902 Y132.981 E311.42513	G1 X58.902 Y132.981 E35.88278	G1 X58.902 Y132.981 E35.88278
G1 X59.249 Y133.026 E311.4395	G1 X59.249 Y133.026 E35.89715	G1 X59.249 Y133.026 E35.89715
G1 X140.751 Y133.026 E314.78766	G1 X140.751 Y133.026 E39.24531	G1 X140.751 Y133.026 E39.24531
G1 X141.189 Y132.957 E314.80588	G1 X141.189 Y132.957 E39.26353	G1 X141.189 Y132.957 E39.26353
G1 X141.661 Y132.719 E314.8276	G1 X141.661 Y132.719 E39.28525	G1 X141.661 Y132.719 E39.28525
G1 X142.022 Y132.334 E314.84928	G1 X142.022 Y132.334 E39.30693	G1 X142.022 Y132.334 E39.30693
G1 X142.231 Y131.848 E314.87101	G1 X142.231 Y131.848 E39.32866	G1 X142.231 Y131.848 E39.32866
G1 X142.232 Y131.836 E314.8715	G1 X142.232 Y131.836 E39.32915	G1 X142.232 Y131.836 E39.32915
G1 X141.921 Y131.736 F7800	G1 X141.921 Y131.736 F7800	G1 X141.921 Y131.736 F7800
;TYPE:External perimeter	;TYPE:External perimeter	;TYPE:External perimeter
G1 F1800	G1 F1800	G1 F1800
G1 X141.947 Y131.501 E314.88121	G1 X141.947 Y131.501 E39.33886	G1 X141.947 Y131.501 E39.33886
G1 X141.947 Y64.911 E317.61678	G1 X141.947 Y64.911 E42.07443	G1 X141.947 Y64.911 E42.07443
G1 X145.553 Y64.911 E317.76492	G1 X145.553 Y64.911 E42.22257	G1 X145.553 Y64.911 E42.22257
G1 X145.553 Y66.714 E317.83899	G1 X145.553 Y66.714 E42.29664	G1 X145.553 Y66.714 E42.29664
G1 X145.553 Y134.858 E320.63839	G1 X145.553 Y134.858 E45.09604	G1 X145.553 Y134.858 E45.09604

Figure 11: *Example of our translation model converting Sailfish G-code to Marlin G-code*